Published by Institute of Physics Publishing for SISSA
Received: *February 8, 2005*
Revised: *May 31, 2005*
Accepted: *June 16, 2005*
Published: *July 15, 2005*

Contrasting supersymmetry and universal extra dimensions at the CLIC multi-TeV e^+e^- collider

Marco Battaglia
Dept. of Physics, University of California, Berkeley, CA 94720, U.S.A., and
Lawrence Berkeley National Laboratory, Berkeley, CA 94720, U.S.A.
E-mail: MBattaglia@lbl.gov

AseshKrishna Datta
MCTP, University of Michigan, Ann Arbor, MI 48109-1120, U.S.A.
E-mail: asesh@umich.edu

Albert De Roeck
CERN, Geneva, Switzerland
E-mail: Albert.de.Roeck@cern.ch

Kyoungchul Kong
Physics Dept., University of Florida, Gainesville, FL 32611, U.S.A.
E-mail: kong@phys.ufl.edu

Konstantin T. Matchev
Physics Dept., University of Florida, Gainesville, FL 32611, U.S.A.
E-mail: matchev@phys.ufl.edu

Abstract: Universal extra dimensions and supersymmetry have rather similar experimental signatures at hadron colliders. The proper interpretation of an LHC discovery in either case may therefore require further data from a lepton collider. In this paper we identify methods for discriminating between the two scenarios at the linear collider. We study the processes of Kaluza-Klein muon pair production in universal extra dimensions in parallel to smuon pair production in supersymmetry, accounting for the effects of detector resolution, beam-beam interactions and accelerator induced backgrounds. We find that the angular distributions of the final state muons, the energy spectrum of the radiative return photon and the total cross-section measurement are powerful discriminators between the two models. Accurate determination of the particle masses can be obtained both by a study of the momentum spectrum of the final state leptons and by a scan of the particle pair production thresholds. We also calculate the production rates of various Kaluza-Klein particles and discuss the associated signatures.

Keywords: Field Theories in Higher Dimensions, Supersymmetry Phenomenology, Beyond Standard Model, Compactification and String Models.

http://jhep.sissa.it/archive/papers/jhep072005033/jhep072005033.pdf

JHEP07(2005)033

Contents

1. Introduction

Supersymmetry (SUSY) and Extra Dimensions offer two different paths to a theory of new physics beyond the Standard Model (SM). They both address the hierarchy problem, play a role in a more fundamental theory aimed at unifying the SM with gravity, and offer a candidate particle for dark matter, compatible with present cosmology data. If either supersymmetry or extra dimensions exist at the TeV scale, signals of new physics should be found by the ATLAS and CMS experiments at the Large Hadron Collider (LHC) at CERN. However, as we discuss below, the proper interpretation of such discoveries, namely the correct identification of the nature of the new physics signals, may not be straightforward at the LHC and may require the complementary data from an e^+e^- collider. In particular, a multi-TeV collider, such as CLIC [1, 2], would ensure a sensitivity over a broad mass range.

A particularly interesting scenario of TeV-size extra dimensions is offered by the so called Universal Extra Dimensions (UED), originally proposed in [3], where all SM particles are allowed to freely propagate into the bulk. The case of UED bears interesting analogies to supersymmetry,[1] and sometimes has been referred to as "bosonic supersymmetry" [4]. In principle, disentangling UED and supersymmetry appears highly non-trivial at hadron colliders [4–6]. For each SM particle, both models predict the existence of a partner (or partners) with identical interactions. Unfortunately, the masses of these new particles are model-dependent and cannot be used to unambiguously discriminate between the two theories, although a degenerate spectrum might suggest UED while a split spectrum would hint[2] towards SUSY. One would therefore like to have an experimental verification which relies on the fundamental distinctions between the two models.

One of the characteristic features of UED is the presence of a whole tower of Kaluza-Klein (KK) partners, labelled by their KK level n. In contrast, $N = 1$ supersymmetry predicts a single superpartner for each SM particle. One might therefore hope to be able to discover the higher KK modes of UED and, having observed a repetition of the SM particle content at each KK level, prove the existence of extra dimensions. However, there are two significant challenges along this route. First, the masses of the higher KK modes are (roughly) integer multiples of the masses of the $n = 1$ KK partners, and as a result their production cross-sections are kinematically suppressed. Second, they predominantly decay to $n = 1$ KK modes, thus simply contributing a small amount to the inclusive production of $n = 1$ KK particles. Just as in the case of SUSY, because of the unknown momentum carried away by the dark matter candidate at the end of the decay chain, one is unable to reconstruct individual KK resonances. The only exceptions are the level 2 KK gauge bosons, which may appear as high mass dijet or dilepton resonances, when they decay directly to SM fermions through loop suppressed couplings [4, 10–12]. Unfortunately the reach of the LHC is rather limited in this case [13], due to the smallness of these loop-suppressed branching fractions. In addition, even if they are discovered, such resonances can be misinterpreted as ordinary Z' gauge bosons in extended supersymmetric models [13].

The second fundamental distinction between SUSY and *the minimal version of* UED is that supersymmetric extensions of the SM necessarily have extended Higgs sectors leading to additional Higgs and higgsino states in the spectrum. The higgsinos of supersymmetry are in one-to-one correspondence with the $n = 1$ KK partners of the Goldstone bosons and cannot be used for discrimination. The additional Higgs bosons of SUSY are not a robust discriminator either. On the one hand, they may simply escape detection at the LHC: the SUSY parameter space has large portions where the LHC discovers a single (SM-like) Higgs boson and misses the rest of the Higgs spectrum. Alternatively, one may consider UED models with an extended Higgs sector which would mimic the SUSY Higgs phenomenology.

The third and most fundamental distinction between UED and supersymmetry is reflected in the properties of the individual particles: the KK partners have identical spin

[1] More precisely, the phenomenology of the first level ($n = 1$) of Kaluza-Klein modes in UED is very similar to that of $N = 1$ supersymmetric models with somewhat degenerate superpartner spectrum and stable lightest supersymmetric particle (LSP). In what follows we shall use the term "supersymmetry" in this somewhat narrower context.

[2] Notice that the recently proposed little Higgs models with T-parity [7–9] are reminiscent of UED, and their spectrum does not have to be degenerate, so they may still be confused with supersymmetry. Under those circumstances, the methods for discrimination discussed in this paper would still apply.

JHEP07(2005)033

quantum numbers as their SM counterparts, while the spins of the superpartners differ by 1/2 unit. However, spin determinations also appear to be difficult at the LHC (or at hadron colliders in general), where the center of mass energy in each event is unknown. In addition, the momenta of the two dark matter candidates in the event are also unknown. This prevents the reconstruction of any rest frame angular decay distributions, or the directions of the two particles at the top of the decay chains. Recently it has been suggested that a charge asymmetry in the lepton-jet invariant mass distributions from a particular cascade, can be used to discriminate SUSY from the case of pure phase space decays [14]. However, the possibility of discriminating SUSY and UED by this method still needs to be demonstrated.

At the LHC, strong processes dominate the production of both KK modes and superpartners. The resulting signatures involve relatively soft jets, leptons and missing transverse energy [4]. The study in [4] shows that, with 100 fb^{-1} of integrated luminosity, the LHC experiments will be able to cover all of the cosmologically preferred parameter space in UED [15]. However, due to the reasons explained above, the discrimination between UED and supersymmetry may be difficult at the LHC.

In this paper, we focus on the minimal UED model, described in some detail in section 2, and on the Minimal Supersymmetric extension of the Standard Model (MSSM) to study how the two models can be discriminated at a linear collider tunable over a center-of-mass energy range of 1 TeV to 3 TeV. We assume that the LHC will have already observed signals of new physics consistent with either $n = 1$ KK modes in UED or sparticle production in supersymmetry. We concentrate on the relevant questions to be addressed by a post-LHC facility. In section 3 we describe the event simulation and reconstruction adopted in this analysis, while in section 4 we contrast UED with supersymmetry using the example of $\mu^+\mu^-\not{E}$ final state. In section 5 we extend our discussion to other possible final states. Section 6 has our conclusions.

2. The minimal UED model

In its simplest incarnation, the UED model has all the SM particles propagating in a single extra dimension of size R, which is compactified on an S_1/Z_2 orbifold. More complicated versions have also been proposed, motivated by ideas about electroweak symmetry breaking [16], neutrino masses [17, 18], proton stability [19] or the number of generations [20]. A peculiar feature of UED is the conservation of Kaluza-Klein number at tree level, which is a simple consequence of momentum conservation along the extra dimension. However, bulk and brane radiative effects [10−12] break KK number down to a discrete conserved quantity, the so called KK parity, $(-1)^n$, where n is the KK level. KK parity ensures that the lightest KK partners — those at level one — are always pair-produced in collider experiments, similar to the case of supersymmetry models with conserved R-parity. KK parity conservation also implies that the contributions to various precisely measured low-energy observables [21−28] only arise at loop level and are small. As a result, the limits on the scale of the extra dimension, from precision electro-weak data, are rather weak, constraining R^{-1} to be larger than approximately 250 GeV [25]. An attractive feature of UED is the presence of a stable massive particle which can be a cold dark matter candidate [12, 15, 29, 30]. The lightest KK partner (LKP) at level one has negative KK parity and can be stable on cosmological scales. In the minimal model, the LKP is the KK partner of the hypercharge gauge boson [12] and its relic density is generically in the desired range [15]. Kaluza-Klein dark matter offers excellent prospects for direct or indirect detection [30 − 36]. Once the radiative corrections to the Kaluza-Klein masses are properly taken into account [12], the collider phenomenology of the minimal UED model[3] exhibits striking similarities to supersymmetry [4, 38] and represents an interesting and well motivated counterexample which can "fake" supersymmetry signals at the LHC.

In the minimal UED model, the bulk interactions of the KK modes readily follow from the SM lagrangian and contain no unknown parameters other than the mass, M_H, of the SM Higgs boson. In contrast, the boundary interactions, which are localized on the orbifold fixed points, are in principle arbitrary, and thus correspond to new free parameters in the theory. They are in fact renormalised by bulk interactions, and are scale dependent [10]. Therefore, we need an ansatz for their values at a particular scale. Of course, the UED model should be treated only as an effective theory which is valid up to some high scale Λ, at which it is matched to some more fundamental theory. In the minimal UED model the boundary terms are assumed to vanish at the cutoff scale Λ, and are subsequently generated through RGE evolution to lower scales. Thus the minimal UED model has only two input parameters: the size of the extra dimension, R, and the cutoff scale, Λ. The number of KK levels present in the effective theory is therefore ΛR and may vary between a few and ~ 40, where the upper limit corresponds to values of Λ leading to a breakdown of perturbativity below the Λ scale.

3. Event simulation and data analysis

In order to study the discrimination of UED signals from supersymmetry, we have implemented the relevant features of the minimal UED model in the `CompHEP` event generator [39]. The MSSM is already available in `CompHEP` since version 41.10. All $n = 1$ KK modes are incorporated as new particles, with the proper interactions and one-loop corrected masses [12]. The widths can then be readily calculated with `CompHEP` on a case by case basis and added to the particle table. Similar to the SM case, the neutral gauge bosons at level 1, Z_1 and γ_1, are mixtures of the KK modes of the hypercharge gauge boson and the neutral $SU(2)_W$ gauge boson. However, it was shown in [4] that the radiatively corrected Weinberg angle at level 1 and higher is very small. For example, γ_1, which is the LKP in the minimal UED model, is mostly the KK mode of the hypercharge gauge boson. For simplicity, in the code we neglect neutral gauge boson mixing for $n \geq 1$.

In the next section we concentrate on the pair production of level 1 KK muons $e^+e^- \to \mu_1^+\mu_1^-$ and compare it to the analogous process of smuon pair production in supersymmetry: $e^+e^- \to \tilde{\mu}^+\tilde{\mu}^-$. In UED there are two $n = 1$ KK muon Dirac fermions: an $SU(2)_W$ doublet μ_1^D and an $SU(2)_W$ singlet μ_1^S, both of which contribute in eq. (3.1) below (see also figure 1).

[3]For alternative possibilities, see [37].

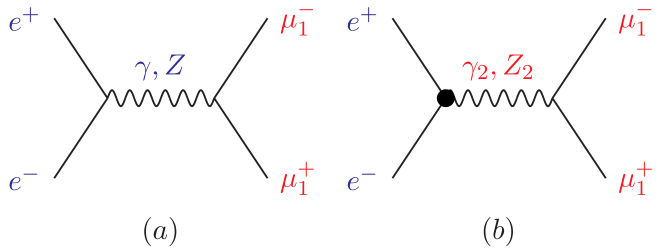

Figure 1: The dominant Feynman diagrams for KK muon production $e^+e^- \to \mu_1^+\mu_1^-$ in Universal Extra Dimensions. The black dot represents a KK-number violating boundary interaction [12].

In complete analogy, in supersymmetry, there are two smuon eigenstates, $\tilde{\mu}_L$ and $\tilde{\mu}_R$, both of which contribute in eq. (3.2). The dominant diagrams in that case are shown in figure 2. In principle, there are also diagrams mediated by γ_n, Z_n for $n = 4, 6, \ldots$ but they are doubly suppressed — by the KK-number violating interaction at both vertices and the KK mass in the propagator — and here can be safely neglected. However, γ_2 and Z_2 exchange (figure 1b) may lead to resonant production and significant enhancement of the cross-section, as well as interesting phenomenology as discussed below in section 4.5. We have implemented the level 2 neutral gauge bosons γ_2, Z_2 with their widths, including both KK-number preserving and the KK-number violating decays as in ref. [4]. We consider the final state consisting of two opposite sign muons and missing energy. It may arise either from KK muon production in UED

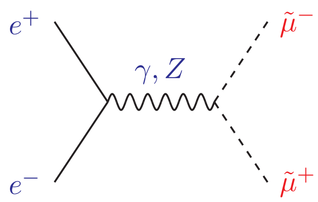

Figure 2: The dominant Feynman diagrams for smuon production $e^+e^- \to \tilde{\mu}^+\tilde{\mu}^-$ in supersymmetry.

$$e^+e^- \to \mu_1^+\mu_1^- \to \mu^+\mu^-\gamma_1\gamma_1\,, \tag{3.1}$$

with γ_1 being the LKP, or from smuon pair production in supersymmetry:

$$e^+e^- \to \tilde{\mu}^+\tilde{\mu}^- \to \mu^+\mu^-\tilde{\chi}_1^0\tilde{\chi}_1^0\,, \tag{3.2}$$

where $\tilde{\chi}_1^0$ is the lightest supersymmetric particle. We reconstruct the muon energy spectrum and the muon production polar angle, aiming at small background from SM processes with minimal biases due to detector effects and selection criteria. The goal is to disentangle KK particle production (3.1) in UED from smuon pair production (3.2) in supersymmetry. We also determine the masses of the produced particles and test the model predictions for the production cross-sections in each case.

Particle	Mass
μ_1^D	515.0 GeV
μ_1^S	505.4 GeV
γ_1	500.9 GeV

Table 1: Masses of the KK excitations for the parameters $R^{-1} = 500\,\mathrm{GeV}$ and $\Lambda R = 20$ used in the analysis.

We first fix the UED parameters to $R^{-1} = 500\,\mathrm{GeV}$, $\Lambda R = 20$, leading to the spectrum given in table 1.

The ISR-corrected signal cross section in UED for the selected final state $\mu^+\mu^-\gamma_1\gamma_1$ is 14.4 fb at $\sqrt{s} = 3\,\mathrm{TeV}$. Events have been generated with `CompHEP` and then reconstructed using a fast simulation based on parametrized response for a realistic detector at CLIC. In particular, the lepton identification efficiency, momentum resolution and polar angle coverage are of special relevance to this analysis. We assume that particle tracks will be reconstructed through a discrete central tracking system, consisting of concentric layers of Si detectors placed in a 4 T solenoidal field. This ensures a momentum resolution $\delta p/p^2$ $= 4.5{\times}10^{-5}\,\mathrm{GeV}^{-1}$. A forward tracking system should provide track reconstruction down to $\simeq 10°$. We also account for initial state radiation (ISR) and for beamstrahlung effects on the center-of-mass energy. We assume that muons are identified by their penetration in the instrumented iron return yoke of the central coil. A 4 T magnetic field sets an energy cutoff of $\simeq 5\,\mathrm{GeV}$ for muon tagging.

The events from the `CompHEP` generation have been treated with the `Pythia 6.210` parton shower [40] and reconstructed with a modified version of the `SimDet 4.0` program [41]. Beamstrahlung has been added to the `CompHEP` generation. The luminosity spectrum, obtained by the `GuineaPig` beam simulation for the standard CLIC beam parameters at 3 TeV, has been parametrised using a modified Yokoya-Chen approximation [42]:

This analysis has backgrounds coming from SM $\mu^+\mu^-\nu\bar{\nu}$ final states, which are mostly due to gauge boson pair production $W^+W^- \to \mu^+\mu^-\nu_\mu\bar{\nu}_\mu$, $Z^0Z^0 \to \mu^+\mu^-\nu\bar{\nu}$ and from $e^+e^- \to W^+W^-\nu_e\bar{\nu}_e$, $e^+e^- \to Z^0Z^0\nu_e\bar{\nu}_e$, followed by muonic decays. The background total cross section is $\simeq 20\,\mathrm{fb}$ at $\sqrt{s} = 3\,\mathrm{TeV}$. In addition to its competitive cross section, this background has leptons produced preferentially at small polar angles, therefore biasing the angular distribution. In order to reduce this background, a suitable event selection has been applied. Events have been required to have two muons, missing energy in excess to 2.5 TeV, transverse energy below 150 GeV and event sphericity larger than 0.05. In order to reject the Z^0Z^0 background, events with di-lepton invariant mass compatible with M_{Z^0} have also been discarded. The underlying $\gamma\gamma$ collisions also produce a potential background to this analysis in the form of $\gamma\gamma \to \mu^+\mu^-$. This background has been simulated using the CLIC beam simulation and `Pythia`. Despite its large cross section, it can be completely suppressed by a cut on the missing transverse energy $E_T^{\mathrm{missing}} > 50\,\mathrm{GeV}$. Finally, in order to remove events with large beamstrahlung, the event sphericity had to be smaller than 0.35 and the acolinearity smaller than 0.8. These criteria provide a factor $\simeq 30$ background suppression, in the kinematical region of interest, while not significantly biasing the lepton momentum distribution.

4. Comparison of UED and supersymmetry in $\mu^+\mu^-\not{E}$

In order to perform the comparison of UED and MSSM, we adjusted the MSSM parameters to get the two smuon masses $M_{\tilde{\mu}_L}$ and $M_{\tilde{\mu}_R}$ and the lightest neutralino mass $M_{\tilde{\chi}_1^0}$ matching exactly those of the two Kaluza-Klein muons $M_{\mu_1^D}$ and $M_{\mu_1^S}$ and of the KK photon M_{γ_1} for the chosen UED parameters. It must be stressed that such small mass splitting between the two muon partners is typically rather accidental in supersymmetric scenarios. The supersymmetric parameters used are given in table 2.

We then simulate both reactions (3.1) and (3.2) with `CompHEP` and pass the resulting events through the same simulation and reconstruction. The ISR-corrected signal cross-

MSSM Parameter	Value
μ	1000 GeV
M_1	502.65 GeV
M_2	1005.0 GeV
$M_{\tilde{\mu}_L}$	512.83 GeV
$M_{\tilde{\mu}_R}$	503.63 GeV
$\tan\beta$	10

Table 2: MSSM parameters for the SUSY study point used in the analysis. This choice of soft SUSY parameters in `CompHEP` leads to an exact match between the corresponding UED and SUSY mass spectra.

section in SUSY for the selected final state $\mu^+\mu^-\tilde{\chi}_1^0\tilde{\chi}_1^0$ is 2.76 fb at $\sqrt{s}$= 3 TeV, which is about 5 times smaller than in the UED case.

4.1 Angular distributions and spin measurements

In the case of UED, the KK muons are fermions and their angular distribution is given by

$$\left(\frac{d\sigma}{d\cos\theta}\right)_{\mathrm{UED}} \sim 1 + \frac{E_{\mu_1}^2 - M_{\mu_1}^2}{E_{\mu_1}^2 + M_{\mu_1}^2}\cos^2\theta\,. \tag{4.1}$$

Assuming that at CLIC the KK production takes place well above threshold, the formula simplifies to:

$$\left(\frac{d\sigma}{d\cos\theta}\right)_{\mathrm{UED}} \sim 1 + \cos^2\theta\,. \tag{4.2}$$

As the supersymmetric muon partners are scalars, the corresponding angular distribution is

$$\left(\frac{d\sigma}{d\cos\theta}\right)_{\mathrm{SUSY}} \sim 1 - \cos^2\theta\,. \tag{4.3}$$

Distributions (4.2) and (4.3) are sufficiently distinct to discriminate the two cases. However, the polar angles θ of the original KK-muons and smuons are not directly observable and the production polar angles θ_μ of the final state muons are measured instead. But as long as the mass differences $M_{\mu_1} - M_{\gamma_1}$ and $M_{\tilde{\mu}} - M_{\tilde{\chi}_1^0}$ respectively remain small, the muon directions are well correlated with those of their parents (see figure 3*a*). In figure 3*b* we show the same comparison after detector simulation and including the SM background. The angular distributions are well distinguishable also when accounting for these effects. By performing a χ^2 fit to the normalised polar angle distribution, the UED scenario considered here could be distinguished from the MSSM, on the sole basis of the distribution shape, with 350 fb^{-1} of data at $\sqrt{s} = 3$ TeV.

4.2 Threshold scans

At the e^+e^- linear collider, the muon excitation masses can be accurately determined through an energy scan of the onset of the pair production threshold. This study not only determines the masses, but also confirms the particle nature. In fact the cross sections for the UED processes rise at threshold $\propto \beta$ while in supersymmetry their threshold onset is $\propto \beta^3$, where β is the particle velocity.

JHEP07(2005)033

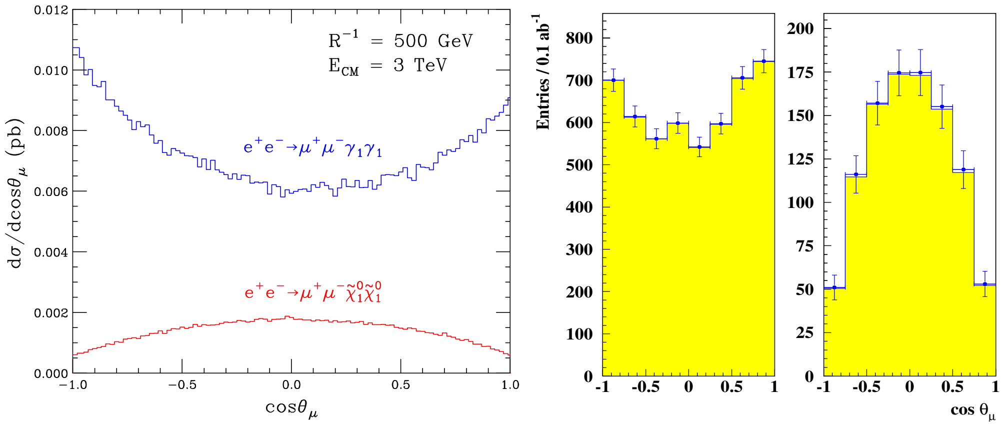

Figure 3: Differential cross-section $d\sigma/d\cos\theta_\mu$ for UED (blue, top) and supersymmetry (red, bottom) as a function of the muon scattering angle θ_μ. The figure on the left shows the ISR-corrected theoretical prediction. The two figures on the right in addition include the effects of event selection, beamstrahlung and detector resolution and acceptance. The left (right) panel is for the case of UED (supersymmetry). The data points are the combined signal and background events, while the yellow-shaded histogram is the signal only.

Since the collision energy can be tuned at properly chosen values, the power rise of the cross section can be tested and the masses of the particles involved measured. We have studied such threshold scan for the $e^+e^- \to \mu_1^+\mu_1^- \to \mu^+\mu^-\gamma_1\gamma_1$ process at $\sqrt{s} = 1\,\text{TeV}$, for the same parameters as in table 1. We account for the anticipated CLIC centre-of-mass energy spread induced both by the energy spread in the CLIC linac and by beam-beam effects during collisions. This been obtained from the detailed `GuineaPig` beam simulation and parametrised using the modified Yokoya-Chen model [42, 43]. An optimal scan of a particle pair production threshold consists of just two energy points, sharing the total integrated luminosity in equal fractions and chosen at energies maximising the sensitivity to the particle widths and masses [44]. For the UED model scan we have taken three points, one for normalisation and two at the maxima of the mass sensitivity (see figure 4). Inclusion of beamstrahlung effects induces a shift of the positions of these maxima towards higher nominal $\sqrt{s}$ values [45]. From the estimated sensitivity $d\sigma/dM$ and the cross section accuracy, the masses of the two UED muon excitations can be determined to $\pm 0.11\,\text{GeV}$ and $\pm 0.23\,\text{GeV}$ for the singlet and the doublet states respectively, with a total luminosity of $1\,\text{ab}^{-1}$ shared in three points, when the particle widths can be disregarded.

4.3 Production cross section determination

The same analysis can be used to determine the cross section for the process $e^+e^- \to \mu^+\mu^- \not{E}$. The SM contribution can be determined independently, using anti-tag cuts, and subtracted. Since the cross section for the UED process at 3 TeV is about five times larger compared to smuon production in supersymmetry, this measurement would reinforce the model identification obtained by the spin determination. This can be quantified by performing the same χ^2 fit to the muon polar production angle discussed above, but now

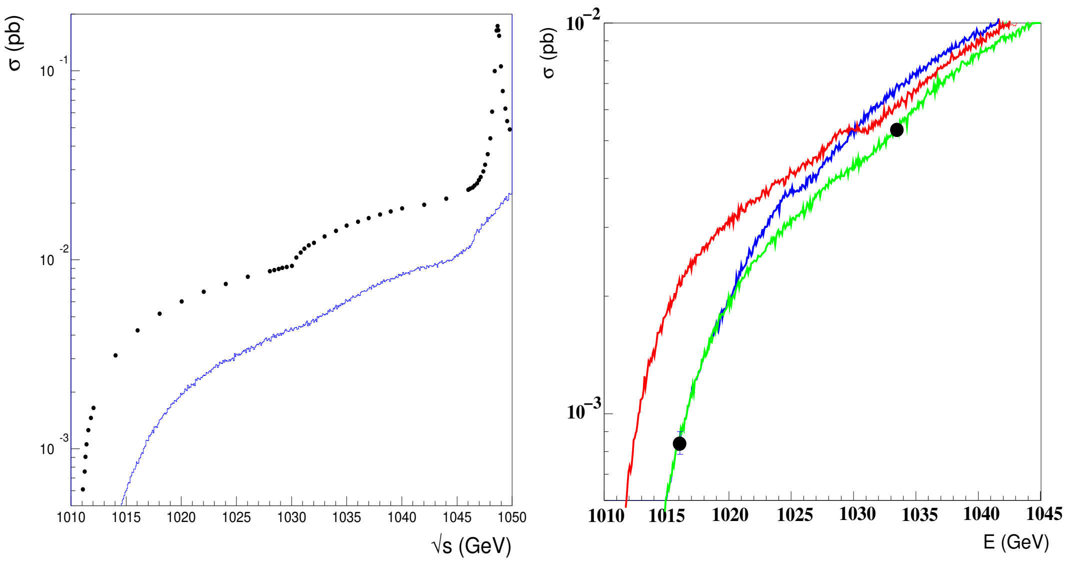

Figure 4: The total $e^+e^- \to \mu_1^+\mu_1^- \to \mu^+\mu^-\gamma_1\gamma_1$ cross section σ in pb as a function of the center-of-mass energy $\sqrt{s}$ near threshold. Left: the threshold onset with (line, blue) and without (dots) beamstrahlung effects. Right: a threshold scan at selected points. The green curve refers to the reference UED parameters while for the red (blue) curve the mass of μ_1^S (μ_1^D) has been lowered by 2.5 GeV. The points indicate the expected statistical accuracy for the cross section determination at the points of maximum mass sensitivity. Effects of the CLIC luminosity spectrum are included.

including also the total number of selected events. Since the cross section depends on the mass of the pair produced particles, we include a systematic uncertainty on the prediction corresponding to a ± 0.05 % mass uncertainty, which is consistent with the results discussed below. At CLIC the absolute luminosity should be measurable to $\mathcal{O}(0.1\ \%)$ and the average effective collision energy to $\mathcal{O}(0.01\ \%)$.

4.4 Muon energy spectrum and mass measurements

The characteristic end-points of the muon energy spectrum are completely determined by the kinematics of the two-body decay and hence they don't depend on the underlying framework (SUSY or UED) as long as the masses involved are tuned to be identical. We show the ISR-corrected expected distributions for the muon energy spectra at the generator level in figure 5*a*, using the same parameters as in figure 3. As expected, the shape of the E_μ distribution in the case of UED coincides with that for MSSM.

The lower, $E_{\rm min}$, and upper, $E_{\rm max}$, endpoints of the muon energy spectrum are related to the masses of the particles involved in the decay according to the relation:

$$E_{\rm max/min} = \frac{1}{2} M_{\tilde\mu} \left(1 - \frac{M^2_{\tilde\chi^0_1}}{M^2_{\tilde\mu}}\right) \gamma(1 \pm \beta) \tag{4.4}$$

where $M_{\tilde\mu}$ and $M_{\tilde\chi^0_1}$ are the smuon and LSP masses and $\gamma = 1/(1-\beta^2)^{1/2}$ with $\beta = \sqrt{1 - M^2_{\tilde\mu}/E^2_{\rm beam}}$ is the $\tilde\mu$ boost. In the case of the UED the formula is completely analogous with M_{μ_1} replacing $M_{\tilde\mu}$ and M_{γ_1} replacing $M_{\tilde\chi^0_1}$.

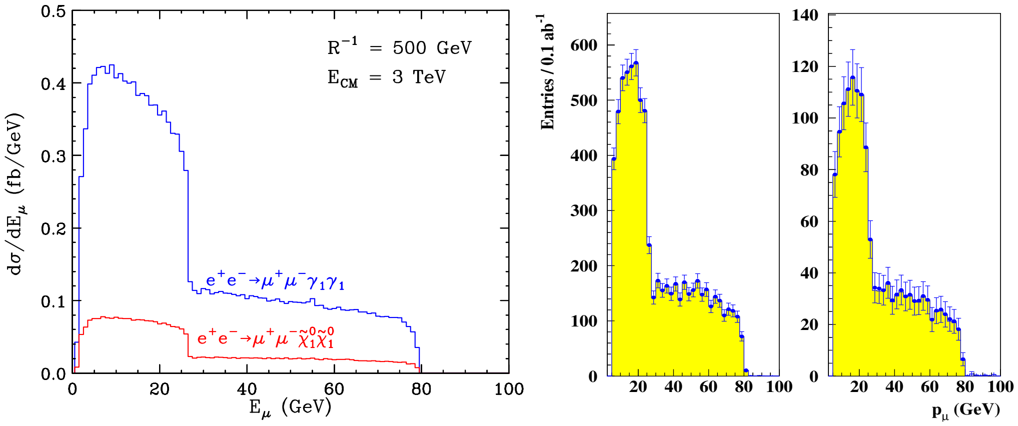

Figure 5: The muon energy spectrum resulting from KK muon production (3.1) in UED (blue, top curve) and smuon production (3.2) in supersymmetry (red, bottom curve). The UED and SUSY parameters are chosen as in figure 3. The plot on the left shows the ISR-corrected distribution, while that on the right includes in addition the effects of event selection, beamstrahlung and detector resolution and acceptance. The data points are the combined signal and background events, while the yellow-shaded histogram is the signal only.

Due to the splitting between the $\tilde{\mu}_L$ and $\tilde{\mu}_R$ masses in MSSM and that between the μ_1^D and μ_1^S masses in UED, in figure 5a we see the superposition of two box distributions. The left, narrower distribution is due to μ_1^S pair production in UED ($\tilde{\mu}_R$ pair production in supersymmetry). The underlying, much wider box distribution is due to μ_1^D pair production in UED ($\tilde{\mu}_L$ pair production in supersymmetry). The upper edges are well defined, with smearing due to beamstrahlung and, but less importantly, to momentum resolution. The lower end of the spectrum has the overlap of the two contributions and with the underlying background. Furthermore, since the splitting between the masses of the μ_1^D, μ_1^S and that of γ_1 is small, the lower end of the momentum distribution can be as low as $\mathcal{O}(1\,\mathrm{GeV})$ where the lepton identification efficiency is cut-off by the solenoidal field bending the lepton before it reaches the electro-magnetic or the hadron calorimeter [46]. Nevertheless, there is sufficient information in this distribution to extract the mass of the γ_1 particle, using the prior information on the μ_1^D and μ_1^S masses, obtained by the threshold scan.

In figure 5b we show the muon energy distribution after detector simulation. A one parameter fit gives an uncertainty on the γ_1 mass of $\pm 0.19\,(\mathrm{stat.}) \pm 0.21\,(\mathrm{syst})\,\mathrm{GeV}$, where the statistical uncertainty is given for $1\,\mathrm{ab}^{-1}$ of data and the systematics reflects the effect of the uncertainty on the μ_1 masses. The beamstrahlung introduces an additional systematics, which depends on the control of the details of the luminosity spectrum.

4.5 Photon energy spectrum and radiative return to the Z_2

With the e^+e^- colliding at a fixed centre-of-mass energy above the pair production threshold a significant fraction of the KK muon production will proceed through radiative return. Since this is mediated by s-channel narrow resonances, a sharp peak in the photon energy spectrum appears whenever one of the mediating s-channel particles is on-shell. In case of

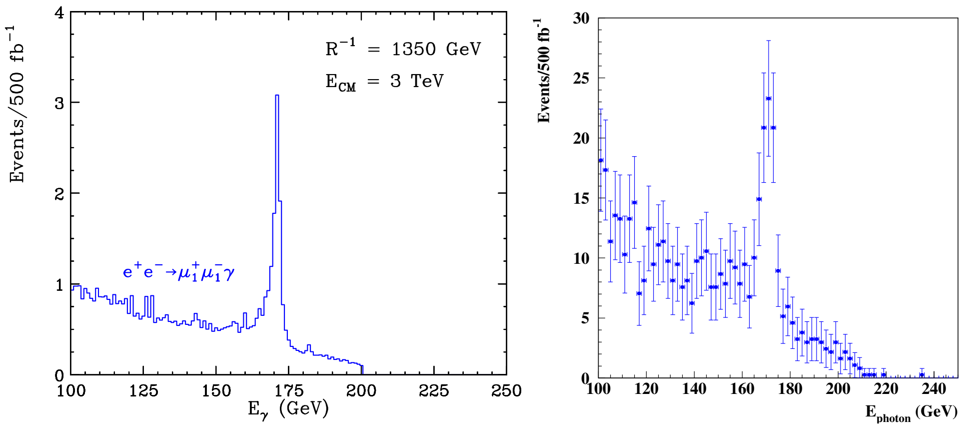

Figure 6: Photon energy spectrum in $e^+e^- \to \mu_1^+\mu_1^-\gamma$ for $R^{-1} = 1350\,\mathrm{GeV}$, $\Lambda R = 20$ and $E_{CM} = 3\,\mathrm{TeV}$ before (left) and after (right) detector simulation. The acceptance cuts are $E_\gamma > 10\,\mathrm{GeV}$ and $1 < \theta_\gamma < 179°$. The mass of the Z_2 resonance is $2825\,\mathrm{GeV}$.

supersymmetry, only Z and γ particles can mediate smuon pair production and neither of them can be close to being on-shell. On the contrary, an interesting feature of the UED scenario is that μ_1 production can be mediated by Z_n and γ_n KK excitations (for n even) as shown in figure 1*b*. Among these additional contributions, the Z_2 and γ_2 exchange diagrams are the most important. Since the decay $Z_2 \to \mu_1\mu_1$ is allowed by phase space, there will be a sharp peak in the photon spectrum, due to a radiative return to the Z_2. The photon peak is at

$$E_\gamma = \frac{1}{2}\,E_{CM}\left(1 - \frac{M_{Z_2}^2}{E_{CM}^2}\right). \tag{4.5}$$

On the other hand, $M_{\gamma_2} < 2M_{\mu_1}$, so that the decay $\gamma_2 \to \mu_1\mu_1$ is closed, and therefore there is no radiative return to γ_2. Notice that the level 2 Weinberg angle is very small [12] and therefore Z_2 is mostly W_2^0-like and couples predominantly to μ_1^D and not μ_1^S.

The photon energy spectrum in $e^+e^- \to \mu_1^+\mu_1^-\gamma$ for $R^{-1} = 1350\,\mathrm{GeV}$, $\Lambda R = 20$ and $E_{CM} = 3\,\mathrm{TeV}$ is shown in figure 6. On the left we show the ISR-corrected theoretical prediction from `CompHEP` while the result on the right in addition includes detector and beam effects. It is clear that the peak cannot be missed.

5. Prospects for discovery and discrimination in other final states

Previously in section 4 we considered the $\mu^+\mu^-\not{E}$ final state resulting from the pair production of level 1 KK muons. However, this is not the only signal which could be expected in the case of UED. Due to the relative degeneracy of the KK particles at each level, the remaining $n = 1$ KK modes will be produced as well, and will yield observable signatures. In those cases, the discrimination techniques which we discussed earlier can still be applied, providing further evidence in favor of one model over the other. In this section we compute the cross-sections for some of the other main processes of interest, and discuss how they could be analysed.

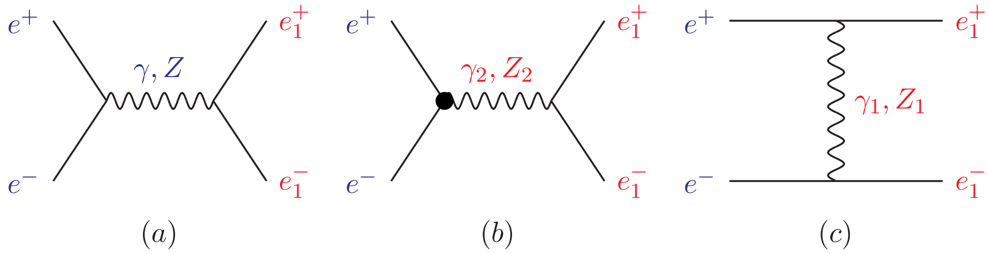

Figure 7: The same as figure 1, but for KK electron production $e^+e^- \to e_1^+e_1^-$.

5.1 Kaluza-Klein leptons

We first turn to the discussion of the other KK lepton flavors. The KK τ-leptons, $\tau_1^\pm$, are also produced in s-channel diagrams only, as in figure 1, hence the $\tau_1^+\tau_1^-$ production cross-sections are very similar to the $\mu_1^+\mu_1^-$ case. The final state will be $\tau^+\tau^-\not{E}$, and it can be observed in several modes, corresponding to the different options for the τ decays. However, due to the lower statistics and the inferior jet energy resolution, none of the resulting channels can compete with the discriminating power of the $\mu_1^+\mu_1^-\not{E}$ final state discussed in the previous section.

The case of KK electrons is more interesting, as it contains a new twist. The production of KK electrons can also proceed through the t-channel diagram shown in figure 7c. As a result, the production cross-sections for KK electrons can be much higher than for KK muons. We illustrate this in figure 8, where we show separately the cross-sections for $SU(2)_W$ doublets (solid lines) and $SU(2)_W$ singlets (dotted lines), as a function of R^{-1}. (For the numerical results throughout section 5, we always fix $\Lambda R = 20$.) At low masses (i.e. low R^{-1}) the $e_1^+e_1^-$ cross-sections can be up to two orders of magnitude larger, compared to the case of $\mu_1^+\mu_1^-$. Another interesting feature is the resonant enhancement of the cross-section for $R^{-1} \sim 1450$ GeV, which is present in either case (e or μ) for the $SU(2)_W$ doublets (solid lines), but not the $SU(2)_W$ singlets (dotted lines). The feature is due to the on-shell production of the level 2 Z_2 KK gauge boson, which can then decay into a pair of level 1 KK leptons (see diagram (b) in figures 1 and 7). Since the Weinberg angle at the higher ($n > 0$) KK levels is tiny [12], Z_2 is predominantly an $SU(2)_W$ gauge boson and hence does not couple to the $SU(2)_W$ singlet fermions, which explains the absence of a similar peak in the e_1^S and μ_1^S cross-sections.[4]

Because of the higher production rates, the $e^+e^-\not{E}$ event sample will be much larger and have better statistics than $\mu^+\mu^-\not{E}$. The $e^+e^-\not{E}$ final state has been recently advertised as a discriminator between UED and supersymmetry in [47]. However, the additional t-channel diagram (figure 7c) has the effect of not only enhancing the overall cross-section, but also distorting the differential angular distributions discussed previously in section 4.1, and creating a forward peak, which causes the cases of UED and supersymmetry to look very much alike. We show the resulting angular distributions of the final state electrons in

[4]One might have expected a second peak closeby due to γ_2 resonant production, but in the minimal UED model the spectrum is such that the decays of γ_2 to level 1 fermions are all closed.

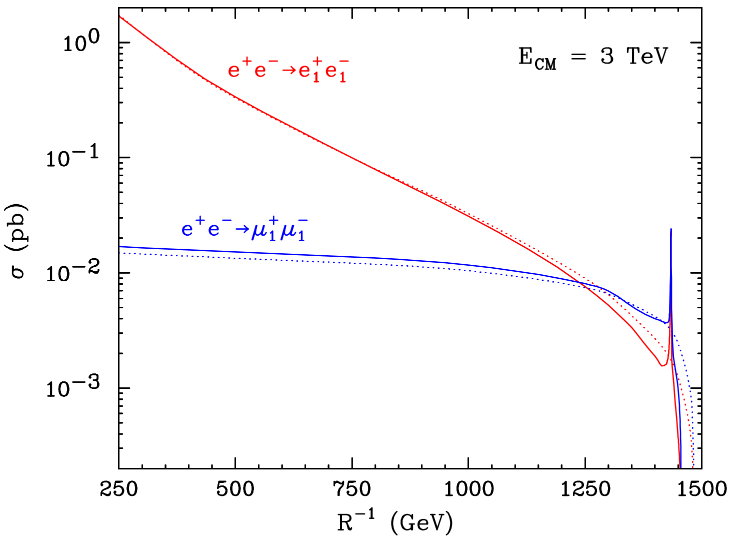

Figure 8: ISR-corrected production cross-sections of level 1 KK leptons (e_1 in red, μ_1 in blue) at CLIC, as a function of R^{-1}. Solid (dotted) lines correspond to $SU(2)_W$ doublets (singlets).

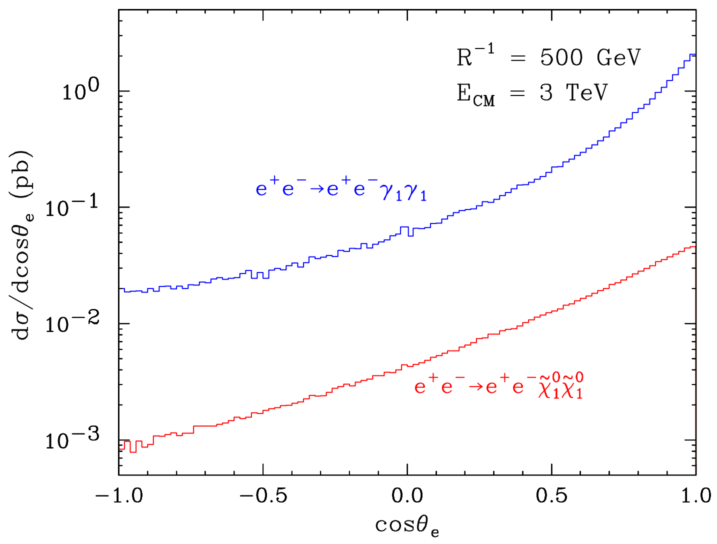

Figure 9: The same as figure 3 (left panel), but for KK electron production $e^+e^- \to e_1^+e_1^-$, with θ_e being the electron scattering angle.

figure 9. For proper comparison, we follow the same procedure as before: we choose the UED spectrum for $R^{-1} = 500$ GeV, which yields KK electron masses as in table 1. We then choose a supersymmetric spectrum with selectron mass parameters as in table 2. This guarantees matching mass spectra in the two cases (UED and supersymmetry) so that any differences in the angular distributions should be attributed to the different spins.

Unlike figure 3, where the underlying shapes of the angular distributions were very distinctive (see eqs. (4.2) and (4.3)), the main effect in figure 9 is the uniform enhancement of the forward scattering cross-section, which tends to wash out the spin correlations exhibited in figure 3.

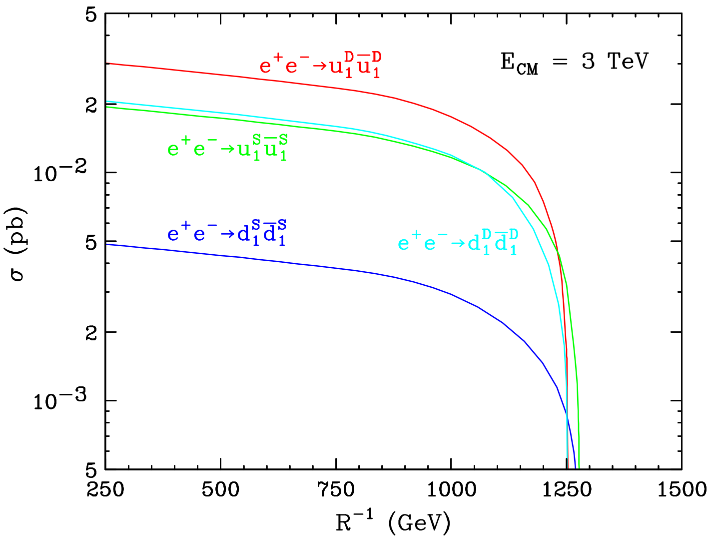

Figure 10: ISR-corrected production cross-sections of level 1 KK quarks at CLIC, as a function of R^{-1}.

5.2 Kaluza-Klein quarks

Level 1 KK quarks will be produced in s-channel via diagrams similar to those exhibited in figure 1. The corresponding production cross-sections are shown in figure 10, as a function of R^{-1}. We show separately the cases of the $SU(2)_W$ doublets u_1^D and d_1^D and the $SU(2)_W$ singlets u_1^S and d_1^S. In the minimal UED model, the KK fermion doublets are somewhat heavier than the KK fermion singlets [12], so naturally, the production cross-sections for u_1^D and d_1^D cut off at a smaller value of R^{-1}. Since singlet production is only mediated by U(1) hypercharge interactions, the singlet production cross-sections tend to be smaller. We notice that $u_1^S\bar{u}_1^S$ is larger by a factor of 2^2 compared to $d_1^S\bar{d}_1^S$, in accordance with the usual quark hypercharge assignments.

The observable signals will be different in the case of $SU(2)_W$ doublets and $SU(2)_W$ singlets. The singlets, u_1^S and d_1^S, decay directly to the LKP γ_1, and the corresponding signature will be 2 jets and missing energy. The jet angular distribution will again be indicative of the KK quark spin, and can be used to discriminate against (right-handed) squark production in supersymmetry, following the procedure outlined in section 4.1. The jet energy distribution will again exhibit endpoints, which will in principle allow for the mass measurements discussed in section 4.4. A threshold scan of the cross-section will provide further evidence of the particle spins (see section 4.2). The only major difference with respect to the $\mu^+\mu^-\not{E}$ final state discussed in section 4, is the absence of the monochromatic photon signal from section 4.5, since Z_2 is too light to decay to KK quarks. In spite of the many similarities to the dimuon final state considered in section 4, notice that jet angular and energy measurements are not as clean and therefore the lepton (muon or electron) final states would still provide the most convincing evidence for discrimination.

The signatures of the $SU(2)_W$ doublet quarks are richer — both u_1^D and d_1^D predominantly decay to Z_1 and $W_1^\pm$ which in turn decay to leptons and the LKP [4]. The analogous process in supersymmetry would be left-handed squark production with subsequent decays

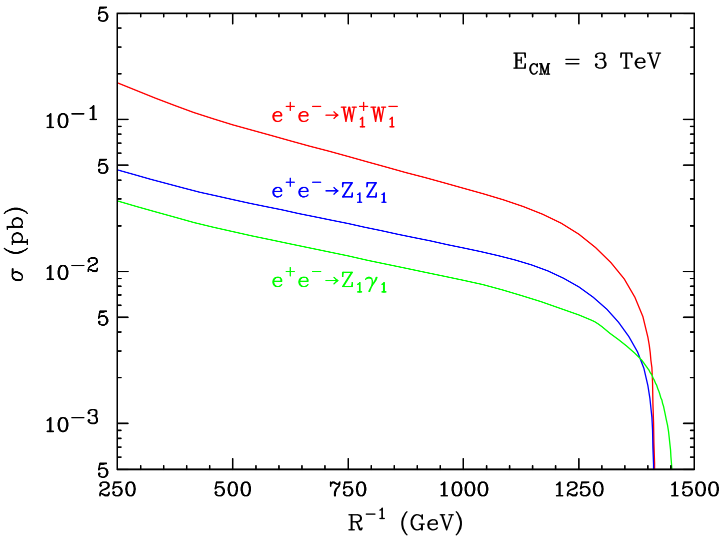

Figure 11: ISR-corrected production cross-sections of level 1 KK gauge bosons at CLIC, as a function of R^{-1}.

to $\tilde{\chi}_2^0$ or $\tilde{\chi}_1^\pm$, which in turn decay to $\tilde{\ell}_L$ and $\tilde{\chi}_1^0$. In principle, the spin information will still be encoded in the angular distributions of the final state particles. However, the analysis is much more involved, due to the complexity of the signature, and possibly the additional missing energy from any neutrinos.

5.3 Kaluza-Klein gauge bosons

The ISR-corrected production cross-sections for level 1 electroweak[5] KK gauge bosons ($W_1^\pm$, Z_1 and γ_1) at a 3 TeV e^+e^- collider are shown in figure 11, as a function of R^{-1}. The three relevant processes are $W_1^+W_1^-$, Z_1Z_1 and $Z_1\gamma_1$ ($\gamma_1\gamma_1$ is unobservable). In each case, the production can be mediated by a t-channel exchange of a level 1 KK lepton, while for $W_1^+W_1^-$ there are additional s-channel diagrams with γ, Z, γ_2 and Z_2. Z_1 and $W_1^\pm$ are almost degenerate [12], thus their cross-sections cut off at around the same point. The analogous processes in supersymmetry would be the pair production of gaugino-like charginos and neutralinos. The final states will always involve leptons and missing energy, since $W_1^\pm$ and Z_1 do not decay to KK quarks.

In conclusion of this section, for completeness we also discuss the possibility of observing the higher level KK particles and in particular those at level 2. For small enough R^{-1}, level 2 KK modes are kinematically accessible at CLIC. Once produced, they will in general decay to level 1 particles and thus contribute to the inclusive production of level 1 KK modes. Uncovering the presence of the level 2 signal in that case seems challenging, but not impossible.

We choose to concentrate on the case of the level 2 KK gauge bosons (V_2), which are somewhat special in the sense that they can decay directly to SM fermions through KK number violating interactions. Thus they can be easily observed as dijet or dilepton

[5]The level 1 KK gluon, of course, has no tree-level couplings to e^+e^-.

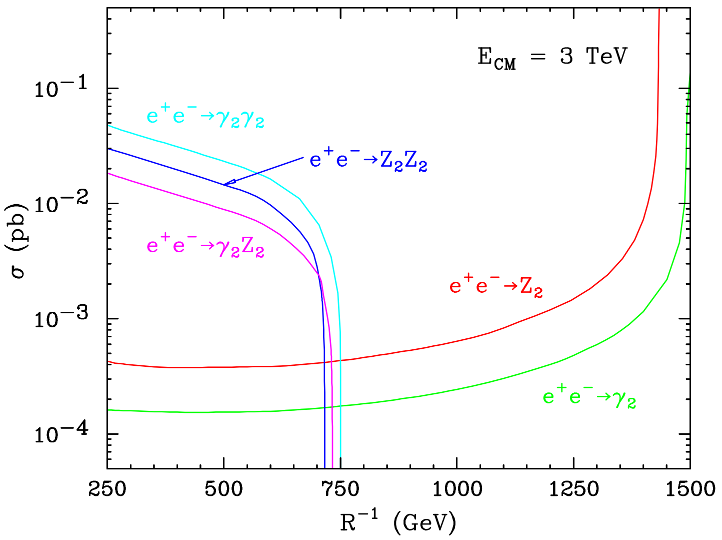

Figure 12: ISR-corrected production cross-sections of level 2 KK gauge bosons at CLIC, as a function of R^{-1}.

resonances. In principle, there are two types of production mechanisms for level 2 gauge bosons. The first is single production $e^+e^- \to V_2$, which can only proceed through KK number violating (loop suppressed) couplings. The second mechanism is $e^+e^- \to V_2V_2$ pair production which is predominantly due to KK number conserving (tree-level) couplings. In figure 12 we show the corresponding cross-sections for the case of the neutral level 2 gauge bosons, as a function of R^{-1}, For low values of R^{-1}, pair production dominates, but as the level 2 gauge boson masses increase and approach E_{CM}, single production becomes resonantly enhanced. Thus the first indication of the presence of the level 2 particles may come from pair production events, but once the mass of the dijet or dilepton resonance is known, the collider energy can be tuned to enhance the cross-section and study the V_2 resonance properties in great detail.

6. Conclusions

Supersymmetry and Universal Extra Dimensions are two appealing examples of new physics at the TeV scale, as they address some of the theoretical puzzles of the SM. They also provide a dark matter candidate which, for properly chosen theory parameters, is consistent with present cosmology data. Both theories predict a host of new particles, partners of the known SM particles. If either one is realised in nature, the LHC is expected to observe signals of these new particles. However, in order to clearly identify the nature of the new physics, one may need to contrast the UED and supersymmetric hypotheses at a multi-TeV e^+e^- linear collider such as CLIC.[6] In this paper we studied in detail the process of pair

[6]Similar studies can also be done at the ILC provided the level 1 KK particles are within its kinematic reach. Since precision data tends to indicate the bound $R^{-1} \geq 250\,\text{GeV}$ for the case of 1 extra dimension, one would need an ILC center-of-mass energy above 500 GeV in order to pair-produce the lowest lying KK states of the minimal UED model.

JHEP07(2005)033

production of muon partners in the two theories, KK-muons and smuons respectively. We used the polar production angle to distinguish the nature of the particle partners, based on their spin. The same analysis could be applied for the case of other KK fermions, as discussed in section 5.

We have also studied the accuracy of CLIC in determining the masses of the new particles involved both through the study of the energy distribution of final state muons and threshold scans. An accuracy of better than 0.1% can be obtained with $1\,\mathrm{ab}^{-1}$ of integrated luminosity. Once the masses of the partners are known, the measurement of the total cross section serves as an additional cross-check on the hypothesized spin and couplings of the new particles. A peculiar feature of UED, which is not present in supersymmetry, is the sharp peak in the ISR photon energy spectrum due to a radiative return to the KK partner of the Z.

The clean final states and the control over the centre-of-mass energy at the CLIC multi-TeV collider allows one to unambiguously identify the nature of the new physics signals which might be emerging at the LHC already by the end of this decade.

Acknowledgments

A.D. is supported by the US Department of Energy and the Michigan Center for Theoretical Physics. The work of A.D., K.K. and K.M. is supported in part by a US Department of Energy Outstanding Junior Investigator award under grant DE-FG02-97ER41209. A.D., K.K. and K.M. acknowledge helpful correspondence with A. Pukhov.

References

[1] The CLIC Study Group, G. Guignard ed., *A 3 TeV e^+e^- linear collider based on CLIC technology*, CERN-2000-008.

[2] C.P.W. Group et al., *Physics at the clic multi-TeV linear collider*, `hep-ph/0412251`.

[3] T. Appelquist, H.-C. Cheng and B.A. Dobrescu, *Bounds on universal extra dimensions*, *Phys. Rev.* **D 64** (2001) 035002 [`hep-ph/0012100`].

[4] H.-C. Cheng, K.T. Matchev and M. Schmaltz, *Bosonic supersymmetry? getting fooled at the LHC*, *Phys. Rev.* **D 66** (2002) 056006 [`hep-ph/0205314`].

[5] T.G. Rizzo, *Probes of universal extra dimensions at colliders*, *Phys. Rev.* **D 64** (2001) 095010 [`hep-ph/0106336`].

[6] C. Macesanu, C.D. McMullen and S. Nandi, *Collider implications of universal extra dimensions*, *Phys. Rev.* **D 66** (2002) 015009 [`hep-ph/0201300`].

[7] H.-C. Cheng and I. Low, *TeV symmetry and the little hierarchy problem*, *JHEP* **09** (2003) 051 [`hep-ph/0308199`].

[8] H.-C. Cheng and I. Low, *Little hierarchy, little higgses and a little symmetry*, *JHEP* **08** (2004) 061 [`hep-ph/0405243`].

[9] J. Hubisz and P. Meade, *Phenomenology of the littlest Higgs with T-parity*, *Phys. Rev.* **D 71** (2005) 035016 [`hep-ph/0411264`].

[10] H. Georgi, A.K. Grant and G. Hailu, *Brane couplings from bulk loops*, *Phys. Lett.* **B 506** (2001) 207 [hep-ph/0012379].

[11] G. von Gersdorff, N. Irges and M. Quiros, *Bulk and brane radiative effects in gauge theories on orbifolds*, *Nucl. Phys.* **B 635** (2002) 127 [hep-th/0204223].

[12] H.-C. Cheng, K.T. Matchev and M. Schmaltz, *Radiative corrections to Kaluza-Klein masses*, *Phys. Rev.* **D 66** (2002) 036005 [hep-ph/0204342].

[13] A. Datta, K. Kong and K. Matchev, in preparation.

[14] A.J. Barr, *Determining the spin of supersymmetric particles at the LHC using lepton charge asymmetry*, *Phys. Lett.* **B 596** (2004) 205 [hep-ph/0405052].

[15] G. Servant and T.M.P. Tait, *Is the lightest Kaluza-Klein particle a viable dark matter candidate?*, *Nucl. Phys.* **B 650** (2003) 391 [hep-ph/0206071].

[16] N. Arkani-Hamed, H.-C. Cheng, B.A. Dobrescu and L.J. Hall, *Self-breaking of the Standard Model gauge symmetry*, *Phys. Rev.* **D 62** (2000) 096006 [hep-ph/0006238].

[17] T. Appelquist, B.A. Dobrescu, E. Ponton and H.-U. Yee, *Neutrinos vis-a-vis the six-dimensional Standard Model*, *Phys. Rev.* **D 65** (2002) 105019 [hep-ph/0201131].

[18] R.N. Mohapatra and A. Perez-Lorenzana, *Neutrino mass, proton decay and dark matter in TeV scale universal extra dimension models*, *Phys. Rev.* **D 67** (2003) 075015 [hep-ph/0212254].

[19] T. Appelquist, B.A. Dobrescu, E. Ponton and H.-U. Yee, *Proton stability in six dimensions*, *Phys. Rev. Lett.* **87** (2001) 181802 [hep-ph/0107056].

[20] B.A. Dobrescu and E. Poppitz, *Number of fermion generations derived from anomaly cancellation*, *Phys. Rev. Lett.* **87** (2001) 031801 [hep-ph/0102010].

[21] K. Agashe, N.G. Deshpande and G.H. Wu, *Can extra dimensions accessible to the SM explain the recent measurement of anomalous magnetic moment of the muon?*, *Phys. Lett.* **B 511** (2001) 85 [hep-ph/0103235].

[22] K. Agashe, N.G. Deshpande and G.H. Wu, *Universal extra dimensions and $b \to s\gamma$*, *Phys. Lett.* **B 514** (2001) 309 [hep-ph/0105084].

[23] T. Appelquist and B.A. Dobrescu, *Universal extra dimensions and the muon magnetic moment*, *Phys. Lett.* **B 516** (2001) 85 [hep-ph/0106140].

[24] F.J. Petriello, *Kaluza-Klein effects on Higgs physics in universal extra dimensions*, *JHEP* **05** (2002) 003 [hep-ph/0204067].

[25] T. Appelquist and H.-U. Yee, *Universal extra dimensions and the Higgs boson mass*, *Phys. Rev.* **D 67** (2003) 055002 [hep-ph/0211023].

[26] D. Chakraverty, K. Huitu and A. Kundu, *Effects of universal extra dimensions on B^0-$\bar{B}^0$ mixing*, *Phys. Lett.* **B 558** (2003) 173 [hep-ph/0212047].

[27] A.J. Buras, M. Spranger and A. Weiler, *The impact of universal extra dimensions on the unitarity triangle and rare K and B decays*, *Nucl. Phys.* **B 660** (2003) 225 [hep-ph/0212143].

[28] A.J. Buras, A. Poschenrieder, M. Spranger and A. Weiler, *The impact of universal extra dimensions on $B \to X_s\gamma$, $B \to X_s$ gluon, $B \to X_s\mu^+\mu^-$, $K_L \to \pi^0 e^+ e^-$ and ϵ'/ϵ*, *Nucl. Phys.* **B 678** (2004) 455 [hep-ph/0306158].

[29] K.R. Dienes, E. Dudas and T. Gherghetta, *Grand unification at intermediate mass scales through extra dimensions*, *Nucl. Phys.* **B 537** (1999) 47 [hep-ph/9806292].

[30] H.-C. Cheng, J.L. Feng and K.T. Matchev, *Kaluza-Klein dark matter*, *Phys. Rev. Lett.* **89** (2002) 211301 [hep-ph/0207125].

[31] D. Hooper and G.D. Kribs, *Probing Kaluza-Klein dark matter with neutrino telescopes*, *Phys. Rev.* **D 67** (2003) 055003 [hep-ph/0208261].

[32] G. Servant and T.M.P. Tait, *Elastic scattering and direct detection of Kaluza-Klein dark matter*, *New J. Phys.* **4** (2002) 99 [hep-ph/0209262].

[33] D. Majumdar, *Detection rates for Kaluza-Klein dark matter*, *Phys. Rev.* **D 67** (2003) 095010 [hep-ph/0209277].

[34] G. Bertone, G. Servant and G. Sigl, *Indirect detection of Kaluza-Klein dark matter*, *Phys. Rev.* **D 68** (2003) 044008 [hep-ph/0211342].

[35] D. Hooper and G.D. Kribs, *Kaluza-Klein dark matter and the positron excess*, *Phys. Rev.* **D 70** (2004) 115004 [hep-ph/0406026].

[36] L. Bergstrom, T. Bringmann, M. Eriksson and M. Gustafsson, *Gamma rays from Kaluza-Klein dark matter*, *Phys. Rev. Lett.* **94** (2005) 131301 [astro-ph/0410359].

[37] C. Macesanu, C.D. McMullen and S. Nandi, *New signal for universal extra dimensions*, *Phys. Lett.* **B 546** (2002) 253 [hep-ph/0207269].

[38] H.-C. Cheng, *Universal extra dimensions at the e^-e^- colliders*, *Int. J. Mod. Phys.* **A 18** (2003) 2779 [hep-ph/0206035].

[39] A. Pukhov et al., *CompHEP: a package for evaluation of Feynman diagrams and integration over multi-particle phase space. User's manual for version 33*, hep-ph/9908288.

[40] T. Sjostrand, L. Lonnblad and S. Mrenna, *Pythia 6.2: physics and manual*, hep-ph/0108264.

[41] M. Pohl and H.J. Schreiber, *SIMDET - version 4: a parametric Monte Carlo for a Tesla detector*, hep-ex/0206009.

[42] M. Peskin, *Consistent Yokoya-Chen approximation to beamstrahlung*, SLAC-TN-04-032.

[43] M. Battaglia, S. Jadach and D. Bardin, *Luminosity determination at CLIC*, in *Proc. of the APS/DPF/DPB summer study on the future of particle physics (Snowmass 2001)*, N. Graf ed., *eConf* **C010630** (2001) E3015.

[44] G.A. Blair, *Sparticle masses and widths via threshold scans at the linear collider*, in *Proc. of the APS/DPF/DPB summer study on the future of particle physics (Snowmass 2001)*, N. Graf ed., SNOWMASS-2001-E3019.

[45] M. Battaglia and M. Gruwe, *Determining the mass of supersymmetric scalars at the clic multi-TeV e^+e^- collider*, hep-ph/0212140.

[46] M. Battaglia, *Particle identification for physics beyond the LHC*, *Nucl. Instrum. Meth.* **A522** (2004) 19 [hep-ex/0311041].

[47] G. Bhattacharyya, P. Dey, A. Kundu and A. Raychaudhuri, *Probing universal extra dimension at the international linear collider*, hep-ph/0502031.

JHEP07(2005)033